Direct Catalytic Conversion of Biomass-Derived Furan and Ethanol to Ethylbenzene

Ivo F. Teixeira,[1] Benedict T.W. Lo,[1] Pavlo Kostetskyy,[2] Lin Ye,[1] Chiu C. Tang,[3] Giannis Mpourmpakis,[2] Shik Chi Edman Tsang[1*]*

[1]Wolfson Catalysis Centre, Department of Chemistry, University of Oxford, OX1 3QR (UK); E-mail: edman.tsang@chem.ox.ac.uk

[2]Department of Chemical Engineering, University of Pittsburgh, Pittsburgh, PA 15261 (USA), E-mail: gmpourmp@pitt.edu

[3]Diamond Light Source Ltd, Harwell Science and Innovation Campus, Didcot, Oxfordshire, OX11 0DE (UK)

Abstract

Herein, we report a synthetic strategy to convert biomass-derived unsubstituted furan to aromatics at high selectivity, especially to ethylbenzene via alkylation/Diels-Alder cycloaddition using ethanol, while greatly reducing the formation of the main side product, benzofuran, over zeolite catalysts. Using synchrotron X-ray powder diffraction and first principles calculations, it is shown that the above methodology favors the formation of aromatic products due to readily alkylation of furan by the first ethanol molecule, followed by Diels-Alder cycloaddition with

derived ethylene from the second ethanol molecule on a Brønsted acid site in a one pot synthesis. This gives a double promoting effect: alkyl substituent(s) on furan creates steric hindrance to inhibit self-coupling to benzofuran while alkylated furan (diene) undergoes Diels-Alder reaction more favorably due to higher HOMO energy.

KEYWORDS: Biomass • Cycloaddition • Zeolite • synchrotron X-ray • Modelling

Introduction

The conversion of lignocellulosic biomass to renewable fuels and chemicals has attracted significant attention as a key technology to enable the replacement of petroleum.[1-2] Lignocellulosic biomass is the most promising renewable carbon energy source, as it is widely available around the world at a relatively low cost.[3] Although it is the most abundant plant material resource, its conversion into chemical faces a range of technological and economic challenges.[4] In order to overcome these challenges, several different processes to obtain chemicals and biofuels from biomass are currently under development.[5-6] The most promising is the multistep strategy using platform molecules as intermediates.[7] Some platform molecules that can be obtained from biomass at good yields are biomass-derived furans, such as furfural, 5-hydroxymethylfurfural (HMF), 2-methylfuran (MF), unsubstituted furan and 2,5-dimethylfuran (DMF), etc.[8]

Furan and 2-methyfuran can be derived from the further conversion of furfural. Furan is obtained from furfural decarbonylation (at 97% yield),[9-10] whereas 2-methylfuran by the direct hydrogenolysis of furfural (at 50% yield)[10] or by its hydrogenation, followed by dehydration of furfuryl alcohol (at 99% overall yield).[3] Many recent studies have reported the Diels-Alder, DA [4+2] cycloaddition reactions between these biomass-derived DMF and MF with ethylene,

followed by dehydration producing aromatics, such as xylene and toluene, respectively.[11-21] It is however, ethylene that is currently produced through non-renewable petroleum routes. Although impressive yields of xylene (90%) and toluene (50%) are achieved from the conversions of DMF and MF, the conversion of unsubstituted furan into benzene or related aromatics gives considerably much lower yield and selectivity. It is primarily due the favorable coupling reaction between two furan molecules, which forms benzofuran (see Scheme 1). Chang et al. reported only 5% of selectivity to benzene at 250 °C by Zr-BEA zeolite catalyst[14] and 35% by BEA zeolite under extremely high pressure of ethylene (62 bar) to enhance the DA rate.[22] They also showed that under 600 °C, the major products from furan conversion are benzofuran and coke (60% carbon selectivity); the benzofuran intermediates can be further converted into aromatics at higher temperatures.[23] However, it is clear that benzofuran is still the inevitable main side product due to the unprotected α-carbon that subjects to side reactions. As a result, the route to obtain ethylbenzene (a styrene precursor) from biomass-derived furan coupling with two ethylene molecules at present is economically non-viable since it is produced at a very low yield.[13]

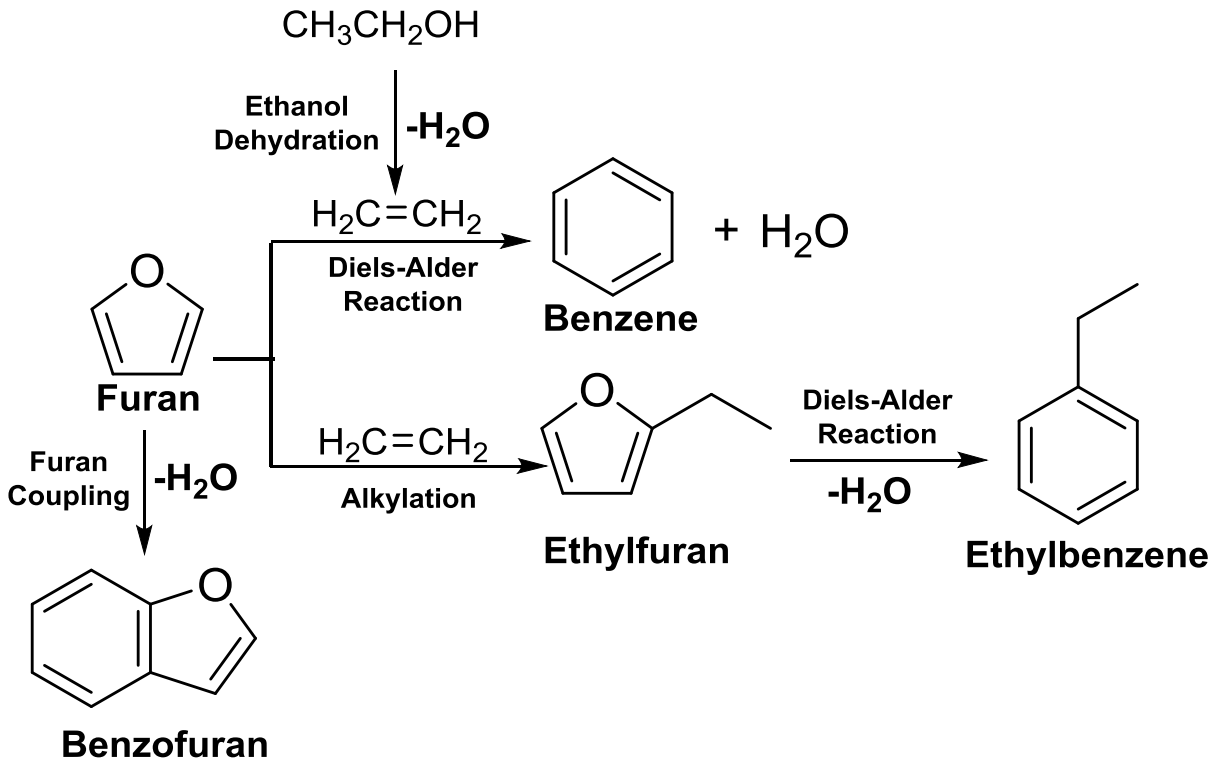

Scheme 1. Furan conversion into aromatics and the side product benzofuran.

Here, we demonstrate the conversion of biomass-derived furan to aromatics, especially to the highly desired product, ethylbenzene using bio-derived ethanol in totally green synthesis rather than ethylene, while greatly attenuating the yield of the side product, benzofuran, over acidic zeolite catalysts. The conversion is based on the DA [4+2] cycloaddition of readily formed ethylfuran intermediate with *in-situ* produced ethylene from ethanol dehydration (ED) in a 'one-pot' solvent-free reaction.

Results and Discussion

First, we compared the catalytic performance of furan with ethanol or ethylene over USY zeolite (Si/Al = 250). Under our optimized reaction conditions, the conversion of furan with ethylene

produces benzofuran as a major product of 63% selectivity (see Fig. 1), followed by benzene 35% and 2% of alkylated aromatics. When the same reaction is performed using ethanol at the same molar ratio, the product selectivity is completely different. The selectivity to benzofuran and alkylated benzofurans is greatly reduced to 23% and the overall selectivity to aromatics is improved to 67%.

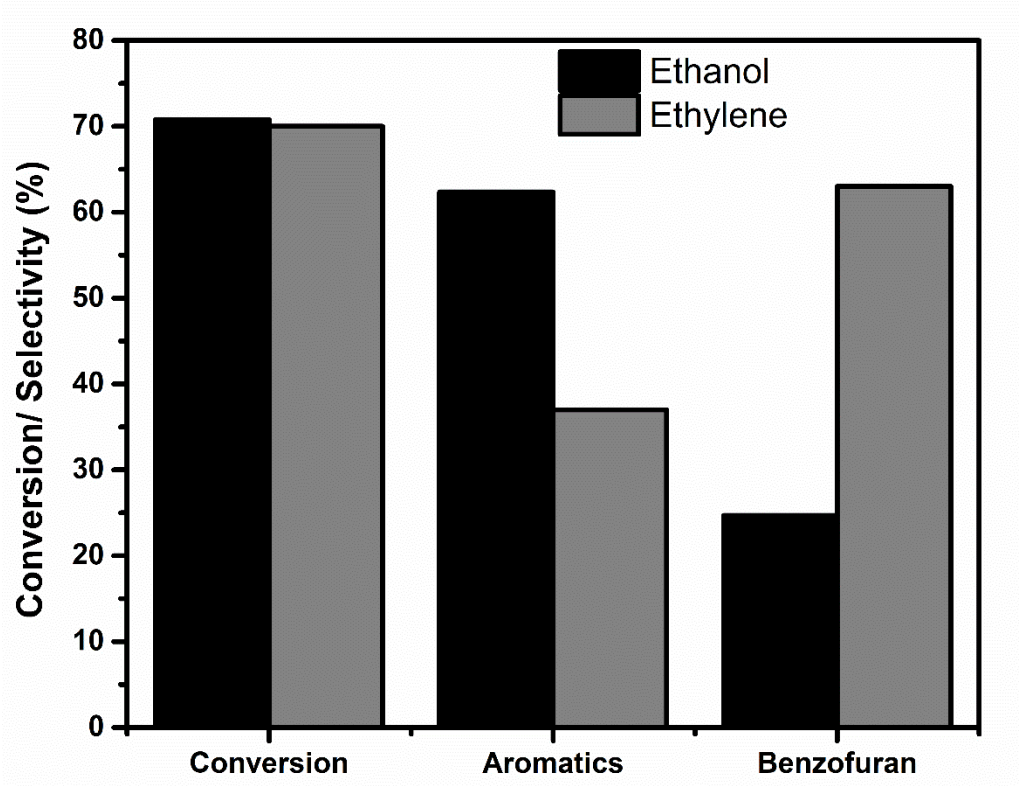

Figure 1. Conversion and selectivity for furan to aromatics catalyzed by zeolite HUSY (Si/Al=250) with ethylene or ethanol, under optimized reaction conditions. Temperature 300 °C, reaction time 8 h, and (black) molar ratio of ethanol to furan of 10:1, (gray) 40 bar of ethylene. All products were quantified, and the carbon balance was achieved at a minimum of 90%.

In Fig.2 the conversion and product distribution for the reaction performed with ethanol (10:1) over HUSY (Si/Al=250) is shown. 70% of the furan was converted with 45% selectivity to

ethylbenzene, 7.9% to diethylbenzene, 14% to other alkylated aromatics (mainly triethylbenzene), 12.5% to ethylfuran and only traces of benzene were detected (around 1%).

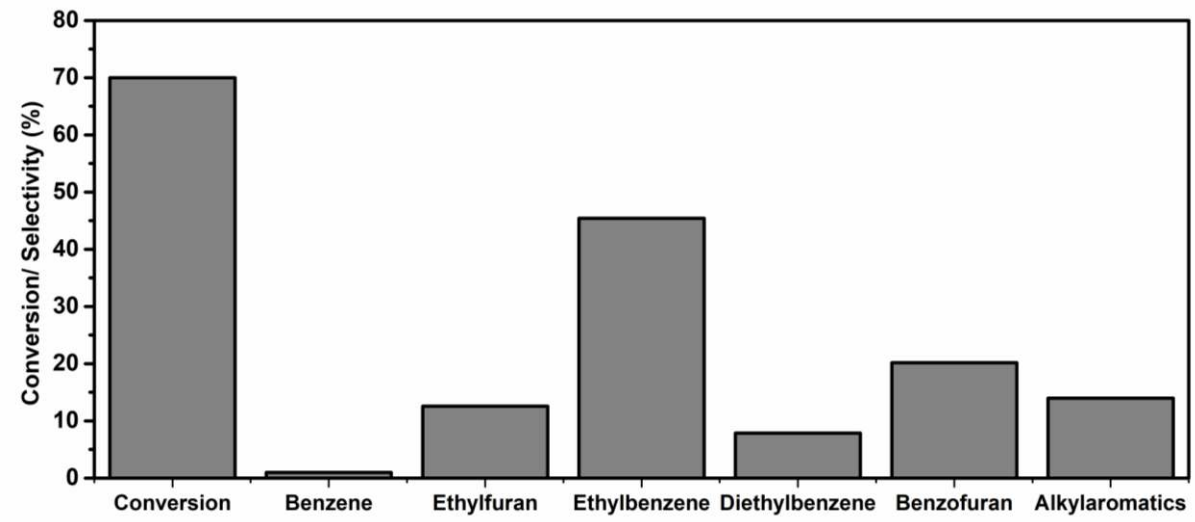

Figure 2. Conversion and selectivity for furan transformation into aromatics catalyzed by 0.4g of zeolite HUSY (Si/Al=250). Reaction conditions: temperature 300 °C, 10:1 Ethanol/Furan molar ratio and reaction time 8 h in 100mL reactor. All products were quantified, and the carbon balance was achieved at a minimum of 90%.

The initial rate of reaction for furan conversion also increases from 0.12 to 0.23 mol g_{cat}^{-1} h^{-1}, when ethanol is used instead of ethylene; but the conversion after prolonged period (e.g. 8 h) converges (ca. 70% for both ethylene and ethanol). Despite the distribution of aromatic products, ethylbenzene remains as the main product which is valuable for the petrochemical industry. Ethylbenzene is generally used to produce styrene for polystyrene synthesis, whereas other alkylated aromatics require a further transalkylation step in order to improve the quality of the aromatic products for other polymers and chemicals processing.[24-25]

It is also found that the catalytic performance is dependent on the framework type and the acidity of the zeolite catalysts (see Table 1, Fig. 3). To decouple these effects, zeolites with similar morphology (Fig. S12) and crystallinity (Fig. S11) were tested. The zeolites with larger pores, i.e. USY and BEA, have more superior aromatic selectivity. Although all the zeolites show much lower selectivity to benzofuran than that reported in literature when ethylene was used,[15, 22] HZSM-5 zeolite still produces benzofuran as the major product. This agrees with the literature that HZSM-5 is a poor catalyst in converting furans into aromatics by the DA reaction.[11] As a typical DA cycloaddition reaction requires a rigid geometric overlap of HOMO-LUMO orbitals, HZSM-5 with smaller pore may not be able to accommodate the spatial needs of the transition state formed between diene and dienophile.

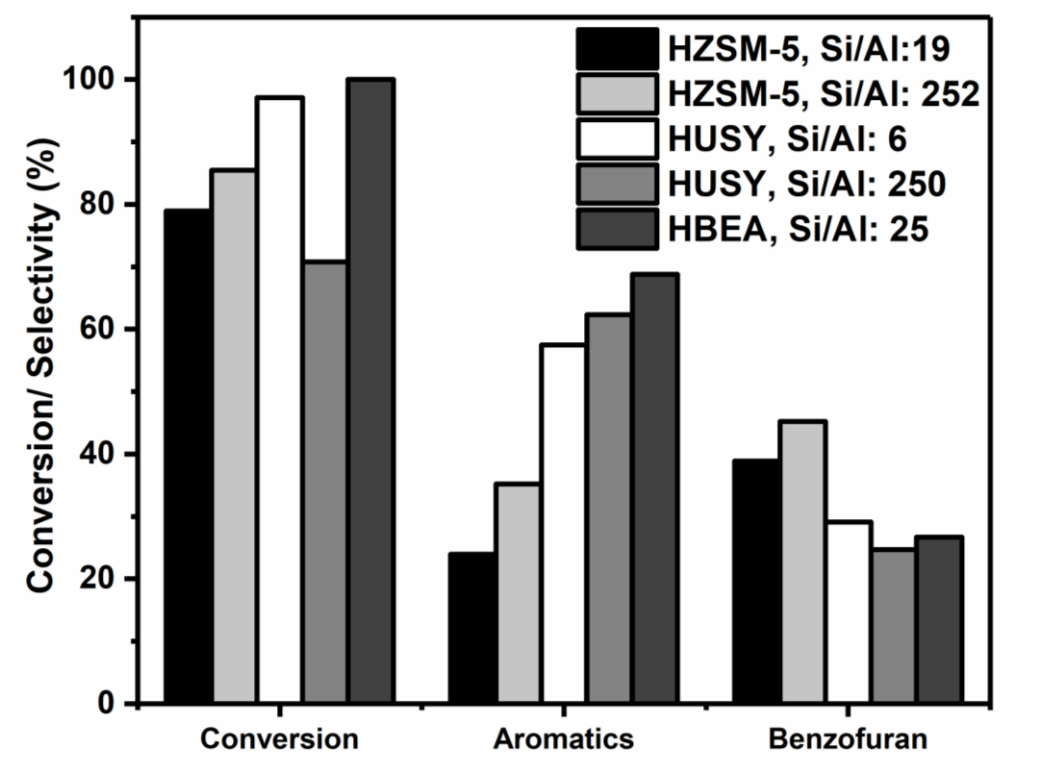

Figure 3. Conversion and selectivity for furan transformation into aromatics catalyzed by different zeolites. Reaction conditions: temperature 300 °C, 0.4 g of catalyst, molar ratio

Ethanol/Furan of 10:1 and reaction time 8 h. All products were quantified, and the carbon balance was achieved at a minimum of 90%.

Table 1. Properties of zeolites and rates of furan conversions

Catalyst	Si/Al ratio[a]	Brønsted acid sites[b] (mmol g^{-1})	Total acid sites[b] (mmol g^{-1})	Surface Area[c] (m^2 g^{-1})	H-TOF[d] (10^2 h^{-1})
HZSM-5	19	0.76	0.789	349	1.3
HZSM-5	252	-	0.002	329	-
HUSY	6	0.55	-	650	11.5
HUSY	250	0.052	-	620	45.7
HBEA	25	0.26	-	575	16.3

[a] from ICP-AES. [b] from ammonia-TPD (there is an on-going debate whether the NH3-TPD technique can differentiate Brønsted acid sites from Lewis acid sites despite the fact that it is still the most commonly used technique to estimate the amount and strength of the acid sites.) [c] from BET over $0.05 < P/P_0 < 0.3$. [d] rate of mol. furan to mol. products per Brønsted acid site per hour.

We have also investigated the effect of acid site concentration in these zeolite catalysts. More acidic zeolites favor higher furan conversion, with 100% conversion catalyzed over HBEA (Si/Al=25) and 97% conversion over HUSY (Si/Al=6). This agrees with our expectation that the furan reactions are likely catalyzed by the BAS of zeolites. The product distribution is also affected by the Brønsted acid concentration, however, it seems to affect in a different degree zeolites with different shapes. For the HZSM-5 zeolites, less acidic samples show higher

selectivity to aromatics, because the more acidic ones tend to produce other side products, such as ketones. Zeolites with USY shape show better selectivity to aromatics when samples with lower acid density are used. The conversion of furan into aromatics over HUSY (Si/Al=250) was optimized in terms of increasing Ethanol/Furan ratio (see Fig. 4).

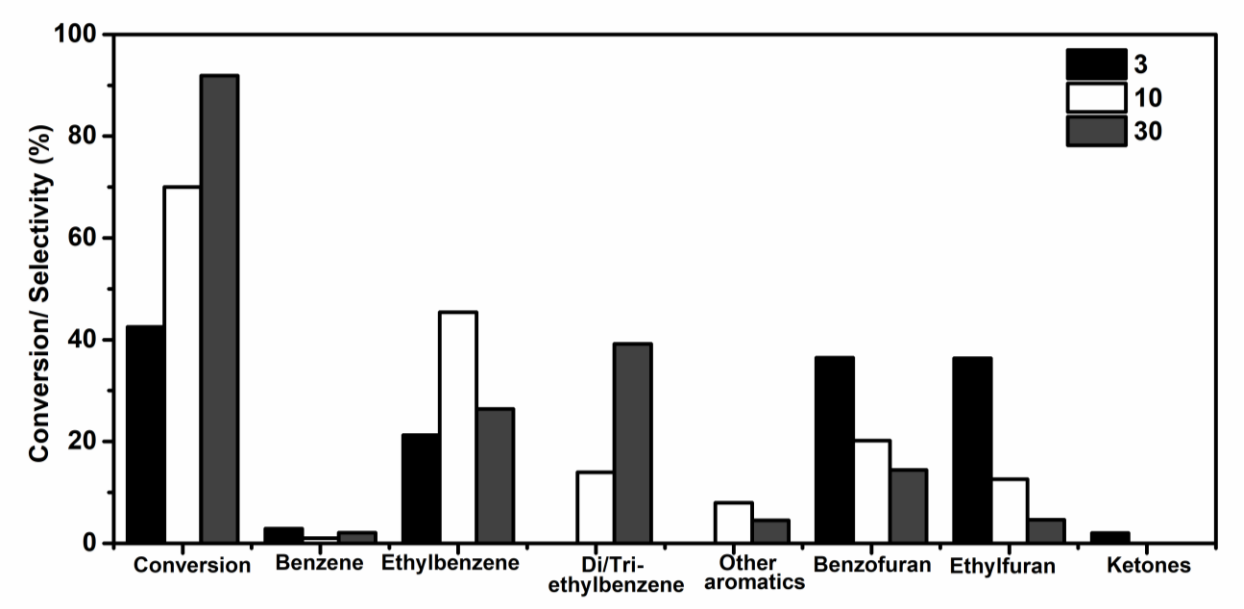

Figure 4. Conversion and selectivity for furan transformation into aromatics catalyzed by 0.4g of zeolite HUSY (Si/Al=250) with different molar ratios Ethanol/Furan. Reaction conditions: temperature 300 °C and reaction time 8 h in 100mL reactor. All products were quantified, and the carbon balance was achieved at a minimum of 90%.

Briefly, a higher Ethanol/Furan ratio gives higher conversion and selectivity toward aromatics. However, the aromatic product distribution is significantly changed; a larger amount of di/tri-ethylbenzene is produced (see Fig. 4). Interestingly, higher molar ratios of Ethanol/Furan further disfavor the formation of benzofuran (undesirable product), reducing its selectivity from 36% to

only 14% when the Ethanol/Furan ratio is increased from 3:1 to 30:1 (see Fig. 4). This may suggest that the reduced coverage of furan on the BAS in favor of ethanol is spatially significant to increase its DA cross-coupling to aromatics at the expense of self-coupling product of benzofuran. However, the competitive replacement of furan by ethanol as a simple site competition model could not account for the significant increase in the overall furan conversions at the increase in the Ethanol/Furan ratios (furan conversion increases from 42% to 92%) and no comparable effect can also be seen by using higher Ethylene/Furan ratios. [15, 22]

Further, we studied the initial production rates for ethylfuran and aromatic products at different Ethanol/Furan ratios (see Fig. 5) in order to gain a better understanding on their relationships.

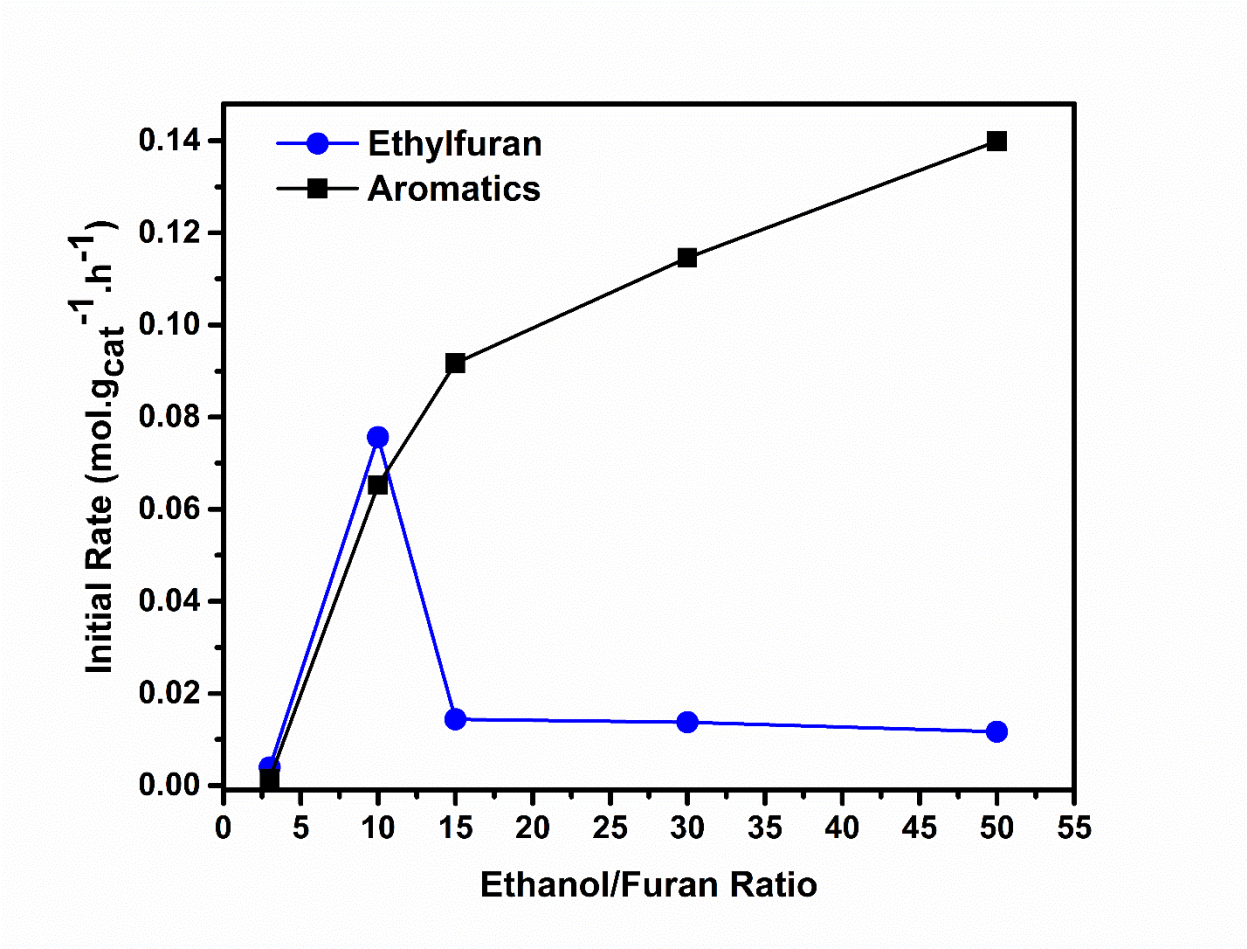

Figure 5. Initial production rate of ethylfuran and aromatics catalyzed by 0.4 g of zeolite HUSY (Si/Al=250) with different molar ratios Ethanol/Furan at 300 °C in a 100 mL reactor.

The initial production rate of ethylfuran rises sharply when the Ethanol/Furan ratio increases from 3:1 to 10:1. However, it declines greatly and stays steadily at low values at the mole ratio of 15:1 to 30:1 probably due to a more favorable conversion of this intermediate to the final aromatics products (see Fig. 5 and Fig. S2). As a result, the production rate of aromatics appears to surpass that of the ethylfuran rate at increasing molar ratios of Ethanol/Furan. A similar trend was observed for the HUSY zeolite (Si/Al=6), the initial rates, however, were an order of magnitude higher. This is likely due to the significant difference in the concentration of Brønsted acid sites (see Fig. S2), cf. 0.55 mmol g^{-1} for the HUSY (Si/Al=6) and 0.052 mmol g^{-1} for the HUSY (Si/Al=250).

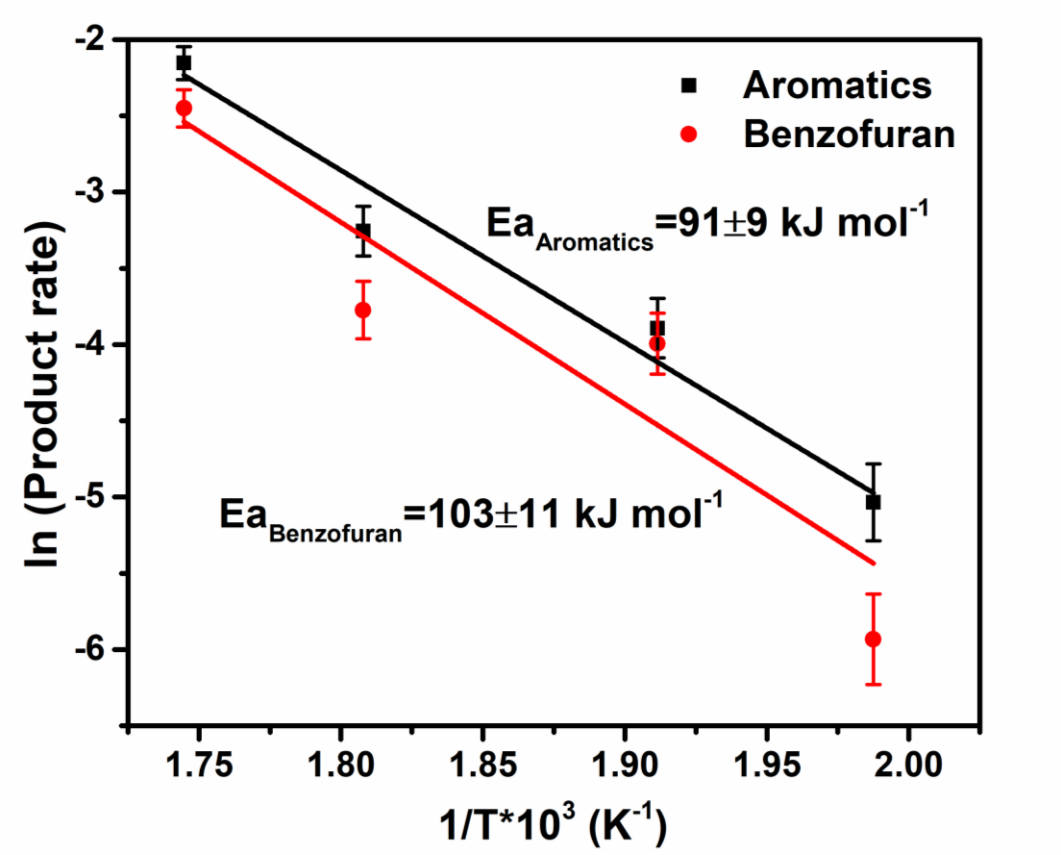

Figure 6. Arrhenius plot for the conversion of furan into aromatics over 0.4 g of HUSY (Si/Al=6) and the estimated activation energies.

HUSY (Si/Al=6) was then chosen for kinetic studies using the Arrhenius plots (see Fig. 6) with the highest initial rate (0.64 mol g_{cat}^{-1} h^{-1}) for the conversion of furan. The apparent activation energy (Ea) is estimated to be 91±9 kJ mol^{-1} for the formation of aromatics, whereas the Ea for benzofuran is 103±11 kJ mol^{-1}. Thus, the formation of benzofuran is more favorable with higher selectivity than that of aromatics as observed experimentally if ethylene is used as the dienophile. Clearly, the use of ethanol can provide an alternative pathway of even lower overall activation energy to couple with furan to aromatics (ethylbenzene) by DA cycloaddition on the BAS as similar to the reported catalytic route to convert ethanol/DMF to xylene.[26]

We have recently developed a synchrotron X-ray powder diffraction (SXRD) combined with Rietveld refinement method to elucidate adsorbate structures in zeolites. The alteration in scattering parameters of modified framework atoms by the molecule(s) enables the probing of adsorption geometries and interactions with the Brønsted acid site in terms of atomic distances and angles, within experimental error.[26-28]

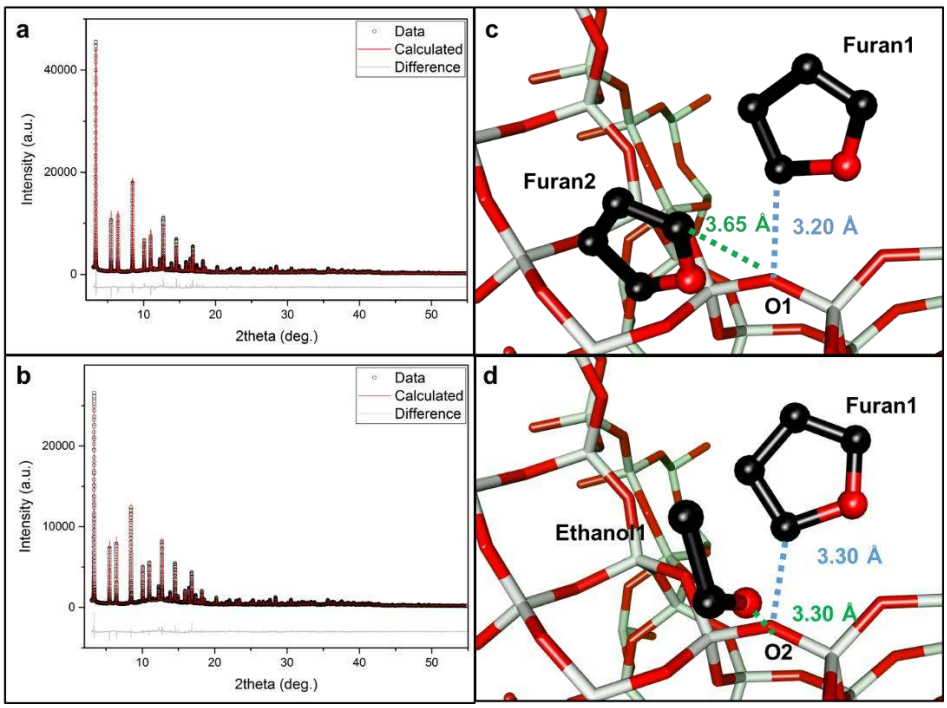

Figure 7. SXRD and Rietveld refinement profiles of (a) furan and 5 bar of ethylene, (b) equimolar of ethanol to furan, (c,d) their corresponding crystal structures showing a fraction of an unit cell for illustration. All the symmetry related molecules are disregarded for clarity. The atomic parameters from Rietveld refinement are summarized in Tables S1-S2 in SI. Atoms are represented in ball/sticks: white = Si/Al, red = O, black = C. No hydrogen atoms are plotted for clarity.

Herein, we applied this SXRD and Rietveld refinement technique to study the fundamental molecular interactions of furan/ethylene or furan/ethanol with BA in the zeolite. The HUSY (Si/Al=6) sample is loaded with a mixture of (i) furan and 5 bar equivalent of ethylene, and (ii) equimolar furan and ethanol. See Fig. 7 (a, b) for the corresponding SXRD and Rietveld refinement profiles, and Fig. S3 for the Rietveld refinement profiles and derived crystal structures of HUSY (Si/Al=6) pre-adsorbed with ethanol and furan at ratios of 3:1 and 10:1 for comparison. As seen in Fig. 7(c), upon the adsorption of ethylene and furan, only furan is

detected. By measuring the closest interatomic distances between furan and the framework oxygen atoms, two furan molecules are co-adsorbed onto the same framework O1 site associated with a T site (BAS) through its electronegative α-carbon; O1-C_{furan1} = 3.20(3) Å and O1-C_{furan2} = 3.65 (3) Å. This 2:1 furan to BAS stoichiometry matches with the similar observation that furan adsorbs in HZSM-5 at a furan-to-aluminum molar ratio of 1.73.[23] Ethylene is much weakly bound on the BAS, which does not compete with furan for protonation; it therefore cannot be detected by SXRD. This may reflect the 'ethyl' carbo-cationic structure formed by protonation of ethylene is intrinsically less stable. Excitingly, upon the adsorption of an equimolar of ethanol and furan, a co-adsorption structure is detected, showing the competition for BAS by the ethanol molecule. The closest interatomic distances between the adsorbates and the HUSY framework: O1-$O_{ethanol}$ (= 3.30(4) Å) and O1-C_{furan} (= 3.30(3) Å), see Fig. 7 (d). Both ethanol and furan appear to interact with the same BAS. It is anticipated that when the Ethanol/Furan ratio increases, more ethanol instead of furan will be protonated on the BAS. Indeed, when more ethanol (with Ethanol/Furan = 3:1 or 10:1, see Fig. S4 and Tables S1-S4) is adsorbed onto the HUSY (Si/Al = 6) sample, a much higher site occupancy of ethanol is detected.

We further investigated the local concentration of ethanol and/or furan, and their corresponding interactions with the BAS for HUSY (Si/Al=6) loaded with Ethanol/Furan ratios of 3:1 and 10:1 using FTIR spectroscopy. The IR spectrum for the sample loaded with 3:1 Ethanol/Furan (Fig. S5) shows characteristic bands for adsorbed ethanol and furan; for ethanol: 2978 cm^{-1} (C-H stretching), 1448 cm^{-1} (-CH_3 degenerate bending) and 1395 cm^{-1} (-CH_3 symmetric bending);[29] for furan: 1468 and 1478 cm^{-1} (ring stretching (adsorbed)) and 1460 and 1490 cm^{-1} (ring stretching (free)).[30] Apparently, the IR data corroborates with the SXRD observations, which also show a co-existence of adsorbed ethanol and furan species in the HUSY. In contrast, for the

10:1 Ethanol/Furan sample, aside from the same characteristic bands for adsorbed ethanol, new bands related with free ethanol molecules are also observed at 2980 cm^{-1} (C-H stretching), 1455 cm^{-1} (-CH_3 degenerate bending) and 1380 cm^{-1} (-CH_3 symmetric bending).[31] Whereas, most of the furan bands at this molar ratio are too small to be identified, apart from the band 1490 cm^{-1} related with free furan molecule. Thus, the FTIR confirms that under higher molar ratios of Ethanol/Furan, ethanol is preferentially protonated, whereas under large excess of ethanol, free ethanol is also present inside the zeolite pores, thus increases the ethanol local concentration.

The above may support the site competition model at higher Ethanol/Furan ratios, such that limited adsorbed furan couples with excess ethanol to give first order rate with respect to furan concentration (see Fig. S6). However, the dramatic inhibition effect for benzofuran formation and the subtle rate enhancement in furan conversion particularly to ethylbenzene at higher Ethanol/Furan ratios are still unaccountable.

First principle calculations can provide insights into the species adsorption in the HUSY and the detailed reaction energy profiles of the competing catalytic reactions. First, the adsorption behavior of ethanol, ethylene, furan, and their mixtures in the pores of the zeolite were modelled using the ONIOM method (see computational details in the SI). It is demonstrated that ethanol binds on the BAS more strongly than furan or ethylene, with binding energies of -65.7, -26.0 and -24.4 kJ mol^{-1}, respectively. It is consistent the same trend of their calculated proton affinities in gas phase (see Tables S5-S6 and Fig. S8). Furan is weakly adsorbed, compared to strongly adsorbed ethanol, which indicates the steric hindrance of furan adsorption into the pore of the HUSY zeolite. Additionally, the strong co-adsorption of the ethanol-furan dimer was also observed within the HUSY model, with a calculated binding energy of -101.5 kJ mol^{-1}, as shown

in Fig. S8(d). This relative adsorption preference of ethanol over furan and particular the formation of ethanol-furan dimer agrees with our experimental SXRD data.

Furthermore, electronic and Gibbs free energies were calculated using density functional theory (DFT) to elucidate the energetically-preferred mechanisms in the network of competing reaction pathways as displayed in Scheme 1 and computational details in SI (Figs. S7, S9, S10). The competing reactions produce desired aromatic products such as benzene and ethylbenzene, as well as undesired furan derivatives (ethylfuran, benzofuran, etc.). The desired aromatic pathways involve DA cycloaddition reactions between the furan or ethylfuran (diene) and ethylene (dienophile). Typically, the intermediates in these reactions are bicyclic oxanorbornene. They readily undergo dehydration to form aromatic products. Recent work on DA chemistry of furans has shown that the rate limiting steps can be dependent on primarily DA cycloaddition step or dehydration step of the cycloadduct intermediate.[11, 26, 32] The undesired derivatives were shown to form by side reactions of furan self-coupling (with additional furan) by DA route (the ring opening route[33] is shown to give higher activation energy, see Fig. 8) and furan alkylation (with ethanol) to ethylfuran.

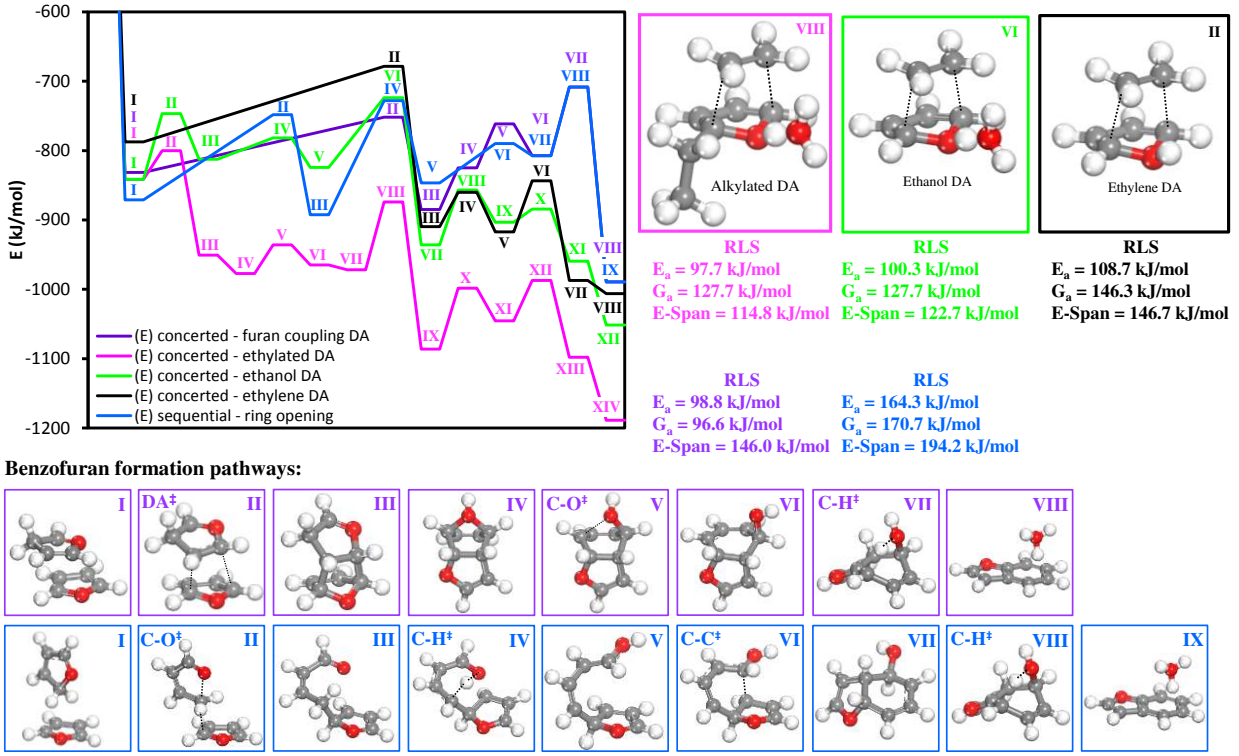

Figure 8. Calculated electronic energies show the energetic profiles of the three DA-limited reactions – ethylated DA, ethanol DA and ethylene DA (magenta, green and black lines, respectively) as well as two benzofuran formation reactions – furan coupling DA and ring opening (purple and blue lines, respectively); RLS stands for rate limiting step.

Similar to our previous work,[26] the interaction of ethanol with the acid site of the zeolite is the key in initiating the formation of aromatic products. For the ethanol-furan reactant pair, we observed a cascade of reactions that was initiated by preferential protonation of ethanol on the BAS. The protonated ethanol can directly react with the neighboring furan ring in dimer to form ethylfuran, exhibiting very low calculated energy barriers (Ea = 41.3 kJ mol^{-1}, Ga = 35.3 kJ mol^{-1}). This elementary step results in the formation of a protonated water molecule (hydronium ion, H_3O^+) as a product, which can form hydrogen bonds with the ethylfuran (diene) and facilitate the

co-adsorption of an additional ethylene molecule (dienophile). Alternatively, the protonated ethanol can dehydrate via concerted elimination to form H_3O^+ and ethylene as the dienophile source produced *in-situ* (Ea = 94.8 kJ mol^{-1}, Ga = 67.1 kJ mol^{-1}). Similar to the case of ethylfuran, the hydronium ion stabilizes (through hydrogen bonding) the ethylene and furan molecules, resulting in a favorable geometric configuration. The subsequent reaction step is the [4+2] DA cycloaddition of the conjugated diene (furans) and dienophile (ethylene) and was shown to be rate-limiting in the BAS-catalyzed reactions, with the corresponding free energies, enthalpies and entropies of rate-limiting barriers involved in the competing mechanisms presented in Fig. 8 and Table 2. The transition state structures of the rate-limiting elementary steps are shown in Fig. S7. Two BAS-catalyzed routes were considered in which H_3O^+ facilitates furan-ethylene (Ethanol DA) and ethylfuran-ethylene (Alkylated DA) interactions. Also, a case of direct DA reaction of protonated furan and ethylene in the absence of water was considered (Ethylene DA). The coupling of two furan molecules to form benzofuran as a side reaction was also evaluated. These calculations were repeated in the absence of the acid catalyst (Uncatalyzed) with the exception of the Ethanol DA pathway, as the ethanol dehydration reaction to produce the dienophile is acid-catalyzed.

Table 2. Elementary reaction barriers calculated for DA steps of relevant pathways in acid-catalyzed and uncatalyzed reactions. Reported values include electronic energies, free energies, enthalpies and entropies at T = 573 K (experimental temperature).

Pathway	**ΔEa (kJ mol^{-1})**	**ΔGa (kJ mol^{-1})**	**ΔHa (kJ mol^{-1})**	**ΔSa (J mol^{-1})**

BAS catalyzed	Alkylated DA	97.7	127.7	95.5	-56.2
	Ethanol DA	100.3	127.7	97.3	-53.0
	Ethylene DA	108.7	146.3	109.8	-63.7
	Furan- Coupling DA	79.5	105.5	75.2	-53.0
Uncatalyzed	Alkylated DA	98.2	136.2	91.9	-77.4
	Ethylene DA	98.7	140.7	92.8	-83.6
	Furan- Coupling DA	144.2	178.5	136.9	-72.5

The DA steps, involving ethylene as the dienophile source, were shown to be practically uncatalyzed by the acidic proton (BAS catalyzed versus uncatalyzed – consistent with previously-published work[26]) and vary minimally in terms of the calculated activation energies (see Table 2). The Alkylated DA and Ethanol DA pathways were shown to be comparable in terms of calculated barriers, with values in near perfect agreement. It suggests that furan alkylation should not hinder cycloaddition reactions. The involvement of additional water molecule in both pathways (produced in ethanol dehydration) decreases the entropic loss at the DA transition state, favoring the Alkylated DA and Ethanol DA pathways (see Table 2 entropy (S) and free energy (G) values). In addition, the enthalpic barrier for the DA step of the Alkylated DA pathway relative to the Ethylene DA pathway was shown to decrease by 14.3 kJ/mol. The furan coupling pathway (Fig. S7(d)) was actually shown to be catalyzed by the BAS of the zeolite and exhibit favorable DA cycloaddition barriers (Ea = 79.5 kJ mol^{-1}, Ga = 105.8 kJ mol^{-1}), catalyzed by the acidic proton, bound on the α-carbon of the (dienophile) furan ring. It thus lowers the HOMO(diene)-LUMO(dienophile) gap from 0.19 to 0.14 Hartree from

uncatalyzed to protonated Furan Coupling DA (Fig. S9). The energy difference of the frontier orbitals involved in the DA reactions was shown to corroborate with the reaction barriers in literature.[11, 26, 32] However, the rate-limiting step in the furan coupling pathway was found to be the water formation step during the dehydration of the cycloadduct intermediates, formed via DA reactions, with the calculated electronic and free energy barriers of Ea = 98.8 kJ mol^{-1} and Ga = 96.6 kJ mol^{-1}, respectively (Fig. 8, blue curve). In contrast, the oxanorbornene intermediates formed in all other pathways are known to readily dehydrate to the aromatic products in the presence of BAS [11, 26, 32] and evolve via sequential C-O and C-H cleavage reactions.

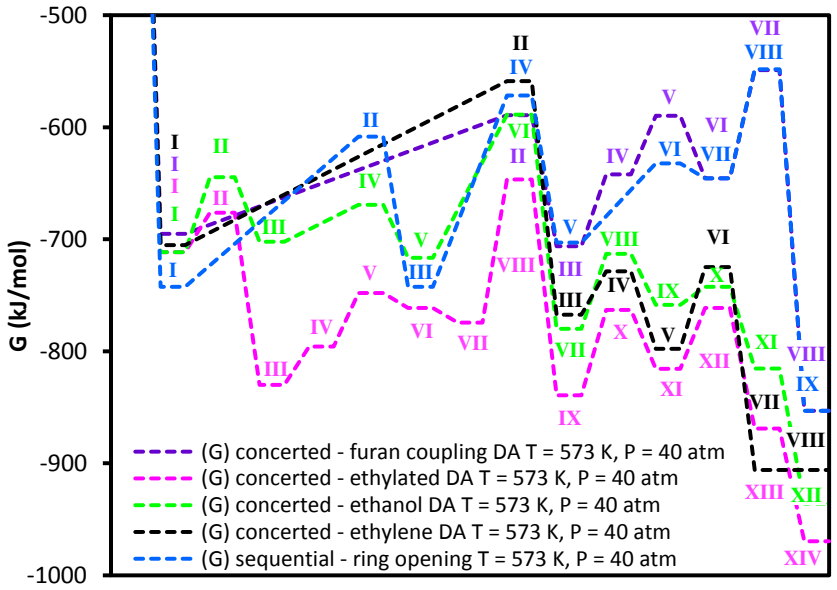

Figure 9: Calculated Gibbs free energies profiles of the three DA-limited reactions – ethylated DA, ethanol DA and ethylene DA (magenta, green and black lines, respectively) as well as two benzofuran formation reactions – furan coupling DA and ring opening (purple and blue lines, respectively); RLS stands for rate limiting step.

In addition to the rate-limiting reaction energy barriers calculated for all pathways, the energetic span model of Kozuch et al.[34] was used to evaluate the kinetics of the reaction system for all the

pathways. It was found that the Alkylated DA pathway was once again favored in terms of the overall energetic span of the reaction, with calculated values of 114.8, 122.7, 146.0, and 146.7 kJ mol^{-1} for the Alkylated DA, Ethanol DA, Furan Coupling and Ethylene DA, respectively. The values of energetic span were calculated using Gibbs free energies of the relevant energetic states (Fig. 9), calculated at the reaction temperature of 573 K, which are comparable to some of our measured values with the same order (Fig. 6). Although the product selectivity trends have been captured by our theoretical calculations, the deviations between the experimentally measured and theoretically calculated barriers can be attributed to the absence of the zeolite pore environment in our reaction pathway calculations.

Thus, the favored and readily pre-alkylation of furan (to ethylfuran) by ethanol on the BAS not only offers steric hindrance for self-furan coupling but notably increases the HOMO energy of the substituted diene in a single pot synthesis.[35] This decreases the HOMO-LUMO energy gap (Fig. S9) that accounts for the faster reaction rate for the Alkylated DA route with the *in-situ* generated ethylene (dienophile), forming corresponding oxabicyclic, which is then rapidly dehydrated into the ethylbenzene product (Scheme 2).

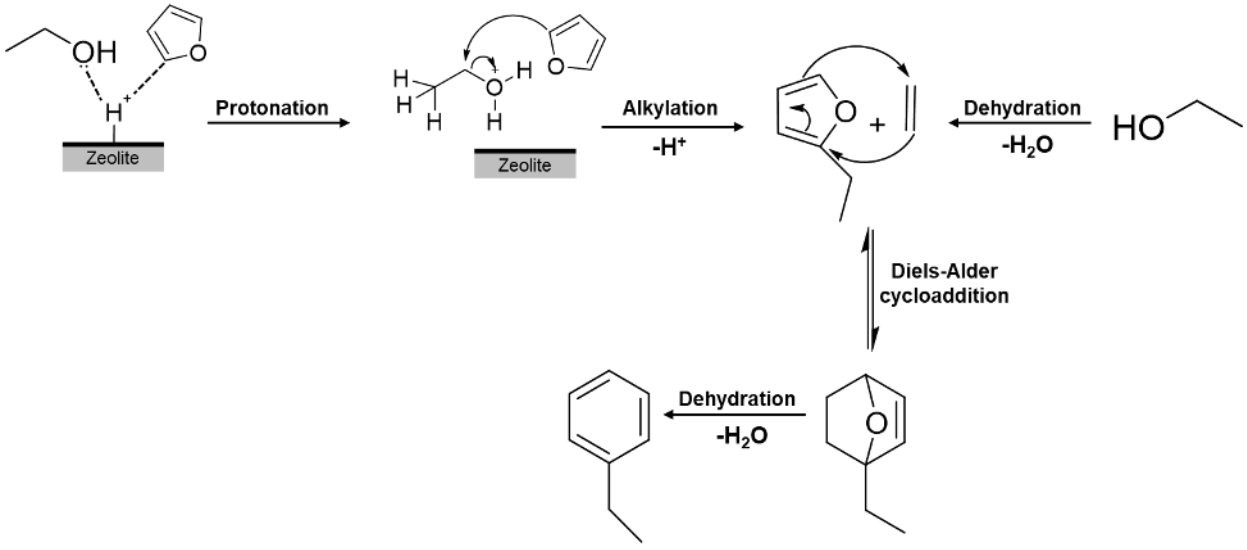

Scheme 2. Furan alkylation, followed by DA cycloaddition and dehydration, catalyzed by the Brønsted acid sites in zeolite catalysts.

Conclusions

In summary, we have demonstrated a valuable biomass conversion strategy into useful products. The zeolite catalysts provide unique and geometrically defined active BAS for a cascade 'one-pot' reactions to form useful aromatics via the DA cycloaddition. The use of ethanol (can also be produced from bio-sources) instead of traditionally used, non-renewable ethylene reduces substantially the formation of the undesired side product – benzofuran. It makes possible *for the first time* the conversion of the important platform molecule, the unsubstituted furan into aromatics, especially the highly desired ethylbenzene, at high yield and selectivity at mild conditions.

ASSOCIATED CONTENT

Supporting Information

Experimental and computational details on the DFT calculations can be found in the supporting information, as well as Figures S1-S10 and Table S1- S6 (PDF).

AUTHOR INFORMATION

Corresponding Authors

*edman.tsang@chem.ox.ac.uk, *gmpourmp@pitt.edu

Author Contributions

The manuscript was written through contributions of all authors. All authors have given approval to the final version of the manuscript.

Notes

The authors declare no competing financial interest. ASSOCIATED CONTENT

Supporting Information

Figures, Tables and relevant discussion with experimental and computational details is available in the supporting information file. This material is available free of charge via the Internet at http://pubs.acs.org.

ACKNOWLEDGMENT

Light Source Ltd (UK) for financial support and IFT is grateful to Brazil CsF/CNPq for a scholarship & YL acknowledges the fellowship from Office of China Postdoctoral Council. PK and GM would like to acknowledge the Donors of the American Chemical Society Petroleum Research Fund (ACS-PRF) and the University of Pittsburgh Center for Research Computing for computational resources. Supporting information for this article is given via a link at the end of the document.

REFERENCES

1. Roman-Leshkov, Y.; Chheda, J. N.; Dumesic, J. A., *Science* **2006,** 312, 1933-7.
2. Wright, M. M.; Roman-Leshkov, Y.; Green, W. H., *Biofuels, Bioprod. Biorefin.* **2012,** 6, 503-520.
3. Alonso, D. M.; Wettstein, S. G.; Dumesic, J. A., *Chem. Soc. Rev.* **2012,** 41, 8075-8098.
4. Singh, N. R.; Delgass, W. N.; Ribeiro, F. H.; Agrawal, R., *Environmental Science & Technology* **2010,** 44, 5298-5305.
5. Huber, G. W.; Iborra, S.; Corma, A., *Chemical reviews* **2006,** 106.

6. Lin, Y.-C.; Huber, G. W., *Energy & Environmental Science* **2009,** 2, 68-80.
7. Luterbacher, J. S.; Martin Alonso, D.; Dumesic, J. A., *Green Chemistry* **2014,** 16, 4816-4838.
8. Zheng, A.; Zhao, Z.; Chang, S.; Huang, Z.; Zhao, K.; Wu, H.; Wang, X.; He, F.; Li, H., *Green Chemistry* **2014,** 16, 2580-2580.
9. Pushkarev, V. V.; Musselwhite, N.; An, K.; Alayoglu, S.; Somorjai, G. A., *Nano Letters* **2012,** 12, 5196-5201.
10. Lange, J. P.; van der Heide, E.; van Buijtenen, J.; Price, R., *ChemSusChem* **2012,** 5, 150-166.
11. Williams, C. L.; Chang, C.-C.; Do, P.; Nikbin, N.; Caratzoulas, S.; Vlachos, D. G.; Lobo, R. F.; Fan, W.; Dauenhauer, P. J., *ACS Catalysis* **2012,** 2, 935-939.
12. Williams, C. L.; Vinter, K. P.; Chang, C.-C.; Xiong, R.; Green, S. K.; Sandler, S. I.; Vlachos, D. G.; Fan, W.; Dauenhauer, P. J., *Catalysis Science & Technology* **2016,** 6, 178-187.
13. Cheng, Y.-T.; Huber, G. W., *Green Chemistry* **2012,** 14, 3114-3114.
14. Chang, C.-C.; Je Cho, H.; Yu, J.; Gorte, R. J.; Gulbinski, J.; Dauenhauer, P.; Fan, W., *Green Chemistry* **2016,** 18, 1368-1376.
15. Wang, D.; Osmundsen, C. M.; Taarning, E.; Dumesic, J. A., *ChemCatChem* **2013,** 5, 2044-2050.
16. Williams, C. L. Production of Sustainable Aromatics from Biorenewable Furans. University of Massachusetts, Amherst, 2014.
17. Rohling, R.; Uslamin, E. A.; Zijlstra, B.; Tranca, I.; Filot, I. A. W.; Hensen, E. J. M.; Pidko, E. A., *ACS Catalysis* **2017**. DOI: 10.1021/acscatal.7b03343
18. Yin, J.; Shen, C.; Feng, X.; Ji, K.; Du, L., *ACS Sustainable Chemistry & Engineering* **2017**. DOI: 10.1021/acssuschemeng.7b03297
19. Rohling, R. Y.; Hensen, E. J. M.; Pidko, E. A., *ChemPhysChem* **2017**. DOI: 10.1002/cphc.201701058
20. Settle, A. E.; Berstis, L.; Rorrer, N. A.; Roman-Leshkov, Y.; Beckham, G. T.; Richards, R. M.; Vardon, D. R., *Green Chemistry* **2017**. DOI: 10.1039/C7GC00992E
21. Li, H.; Riisager, A.; Saravanamurugan, S.; Pandey, A.; Sangwan, R. S.; Yang, S.; Luque, R., *ACS Catalysis* **2017**, 148-187.
22. Chang, C.-C.; Green, S. K.; Williams, C. L.; Dauenhauer, P. J.; Fan, W., *Green Chemistry* **2014,** 16, 585-588.
23. Cheng, Y.-T.; Huber, G. W., *ACS Catalysis* **2011,** 1, 611-628.
24. Gallego, E. M.; Portilla, M. T.; Paris, C.; León-Escamilla, A.; Boronat, M.; Moliner, M.; Corma, A., *Science* **2017,** 355, 1051-1054.
25. Serra, J. M.; Guillon, E.; Corma, A., *Journal of Catalysis* **2004,** 227, 459-469.
26. Teixeira, I. F.; Lo, B. T. W.; Kostetskyy, P.; Stamatakis, M.; Ye, L.; Tang, C. C.; Mpourmpakis, G.; Tsang, S. C. E., **2016**, 13061.
27. Ye, L.; Teixeira, I.; Lo, B. T. W.; Zhao, P.; Edman Tsang, S. C., *Chemical Communications* **2017,** 53, 9725-9728.
28. Ye, L.; Lo, B. T. W.; Qu, J.; Wilkinson, I.; Hughes, T.; Murray, C. A.; Tang, C. C.; Tsang, S. C. E., *Chemical Communications* **2016,** 52, 3422-3425.
29. Kondo, J. N.; Ito, K.; Yoda, E.; Wakabayashi, F.; Domen, K., *The Journal of Physical Chemistry B* **2005,** 109, 10969-10972.
30. Spoto, G.; Geobaldo, F.; Bordiga, S.; Lamberti, C.; Scarano, D.; Zecchina, A., *Topics in Catalysis* **1999,** 8, 279-292.

31. Duan, H. Q.; Yan, R.; Koe, L. C. C.; Wang, X. L., *Chemosphere* **2007,** 66, 1684-1691.
32. Nikbin, N.; Do, P. T.; Caratzoulas, S.; Lobo, R. F.; Dauenhauer, P. J.; Vlachos, D. G., **2013,** 297, 35-43.
33. Vaitheeswaran, S.; Green, S. K.; Dauenhauer, P.; Auerbach, S. M., *ACS Catalysis* **2013,** 3, 2012-2019.
34. Kozuch, S.; Shaik, S., *Acc. Chem. Res.* **2011,** 44, 101-110.
35. John, I. G.; Radom, L., *Journal of the American Chemical Society* **1978,** 100, 3981-3991.

TOC